

Lawrence Berkeley National Laboratory

Chemical Sciences

Title

Nickel Diselenide Ultrathin Nanowires Decorated with Amorphous Nickel Oxide Nanoparticles for Enhanced Water Splitting Electrocatalysis

Permalink

<https://escholarship.org/uc/item/7dt6z60k>

Journal

Small, 13(37)

ISSN

1613-6810

Authors

Li, Haoyi
Chen, Shuangming
Lin, Haifeng
et al.

Publication Date

2017-10-01

DOI

10.1002/smll.201701487

Peer reviewed

Nickel Diselenide Ultrathin Nanowires Decorated with Amorphous Nickel Oxide Nanoparticles for Enhanced Water Splitting Electrocatalysis

Haoyi Li, Shuangming Chen, Haifeng Lin, Xiaobin Xu, Haozhou Yang, Li Song, and Xun Wang*

Well-designed hybrid materials based on noble metal-free elements have great potential to generate hydrogen (H_2) and oxygen (O_2) sustainably via overall water splitting for developing practical energy-related technologies. Herein, an accessible method is presented to synthesize nickel diselenide ($NiSe_2$) ultrathin nanowires decorated with amorphous nickel oxide nanoparticles (NiO_x NPs) as multifunctional electrocatalysts (NSWANs) for hydrogen and oxygen evolution reaction (HER and OER). The NSWANs exhibit quite low HER and OER overpotentials of 174 and 295 mV, respectively, holding the current density of 20 mA cm^{-2} for 24 h continuous operations in alkaline media. Meanwhile, a cell voltage of 1.547 V at the current density of 10 mA cm^{-2} for overall water splitting has been achieved by the NSWANs for the practical application, which could maintain fascinating activity of 20 mA cm^{-2} for 72 h without degradation. The decorated NiO_x NPs not only prevent the $NiSe_2$ from further oxidation but also expose requisite active sites for electrocatalytic process. It is believed that this study may provide a valuable strategy to design high-efficiency electrocatalysts and expand the applications of selenide-based materials.

Along with the crisis of energy consumption and environmental pollution aggravating, exploring alternative and environment-friendly power sources to replace fossil fuels has become considerable research interests for decades.^[1]


Hydrogen (H_2) is regarded as one of the most promising candidates for industrial and social utilization of energy owing to its zero-carbon feature, efficient availability, and high calorificity.^[2] Electrochemical or photo-electrochemical water splitting is a well-established approach with low cost and great efficiency for hydrogen production taking account of bountiful water resources.^[3] However, it is hampered by intrinsic energy barriers of overall water splitting, including two half reactions of hydrogen and oxygen evolution reaction (HER and OER).^[4] Notably, Pt alloys are highly active in HER electrolysis with extremely low overpotentials, and Ir/Ru oxides are the state-of-the-art OER electrocatalysts, but high cost and scarcity hinder the wholesale application of them.^[5] Therefore, a leap-type forward development is needed to discover inexpensive electrocatalysts based on earth-abundant elements with high activity to decrease overpotentials as well as enhance durability for both HER and OER electrocatalysis.

A large quantity of efforts have been devoted to achieving this forward step.^[6] It is noteworthy that transition

H. Y. Li, Dr. H. F. Lin, Dr. X. B. Xu, H. Z. Yang, Prof. X. Wang
Key Lab of Organic Optoelectronics and Molecular Engineering
Department of Chemistry
Tsinghua University
Beijing 100084, China
E-mail: wangxun@mail.tsinghua.edu.cn



Dr. S. M. Chen, Prof. L. Song
National Synchrotron Radiation Laboratory
CAS Center for Excellence in Nanoscience
University of Science and Technology of China
Hefei 230029, China

 The ORCID identification number(s) for the author(s) of this article can be found under <https://doi.org/10.1002/sml.201701487>.

DOI: 10.1002/sml.201701487

metal-based materials, such as hydroxides,^[7] oxides,^[8] sulfides,^[9] nitrides,^[10,11] phosphides,^[12] carbides,^[13] and selenides,^[14] have high activity and long-term stability in electrocatalyzing HER and OER. Among these compounds, pyrite-structured transition metal dichalcogenides (MX_2 ; $\text{M} = \text{Fe}, \text{Co}, \text{Ni}$ and $\text{X} = \text{S}, \text{Se}$) have attracted tremendous attention due to their extraordinary performances of electrocatalysis and photovoltaic devices.^[15] NiSe_2 , benefitting from its unique electronic structure, makes its application in HER electrolysis appealing.^[16] Liang et al. have developed a facile method to synthesize NiSe_2 nanoparticles for catalyzing hydrogen generation with superior kinetics.^[17] The porous NiSe_2 nanosheets were synthesized from $\beta\text{-Ni}(\text{OH})_2$ conversion showing high activity for HER and overall water splitting because of rich edge sites.^[18] Moreover, a recent study illustrates that electrode based on Se-enriched NiSe_2 nanosheet arrays exhibits excellent performance for HER with increased active sites, which are easily accessible to the HER-relevant species.^[19] Nevertheless, applications of NiSe_2 -based nanomaterials can still be further explored because scarcely any researches have reported that they serve as both cathode and anode to facilitate water splitting in the same media. High concentration of H^+ and OH^- could not be provided simultaneously to accelerate HER and OER in one electrolyte because the arithmetic product value of the concentration of H^+ and OH^- is constant in one aqueous solution. If two sorts of catalysts were used in realistic overall water splitting, the complex process of fabricating electrodes would increase the cost. Therefore, NiSe_2 -based electrocatalysts for overall water splitting still need to be deeply studied.

There are two critical points that should be considered for engineering NiSe_2 -based nanomaterials for electrolysis. First, intrinsic catalytic active sites need to be proliferated as many as possible.^[20] Second, the major component should remain stable and be protected from oxidation in the application process.^[10,21] On account of the two factors, in this work, we report an accessible approach to synthesize nickel diselenide ultrathin nanowires (NiSe_2 UNWs) decorated with amorphous nickel oxide nanoparticles (NiO_x NPs) as bifunctional electrocatalysts (NSWANs) for HER and OER. With carbon fiber paper (CFP) as the substrate, the NSWANs have been used to electrocatalyzing overall water splitting within one alkaline electrolyzer. For the hybrid nanostructures, NiO_x NPs play a significant role during the electrolysis, which not only provide more catalytic active sites for HER and OER^[22] but also prevent NiSe_2 from further oxidation. Amorphous materials possess a larger quantity of randomly oriented bonds than the crystalline counterpart. Therefore, more surface unsaturated sites are found, which can improve the adsorption of reactants and result in higher catalytic activity.^[23] Moreover, higher structural flexibility is the characteristic feature of the amorphous structures rather than the crystalline ones. The local structural flexibility is quite significant for the electrocatalytic performances, because the local structure of the adsorption sites is easily distorted by formation of intermediates.^[24] We believe that this study can pave the way to design and fabricate the bifunctional electrocatalysts of overall water splitting for NiSe_2 -based nanomaterials.

The synthetic details are illustrated in the Supporting Information. In our synthesis, NiSe_2 UNWs were synthesized first by a hot-injection method in ethylene glycol system. The as-prepared NiSe_2 UNWs were then characterized by transmission electron microscopy (TEM) and scanning TEM (STEM). As shown in **Figure 1a,b**, these nanowires were uniform with high purity and its length ranged from around 50 to over 500 nm. In the reaction system, polyvinyl pyrrolidone (PVP, $M_w \approx 30\,000$) acted as a structure-directing agent. As compared to the pristine NiSe_2 UNWs, the sample without PVP just exhibited morphology of nanoparticles with some obvious aggregations (Figure S1, Supporting Information). Mutual curling and twining manifested flexibility of NiSe_2 UNWs owing to PVP polymers capping on the surface of the nanowires, which was quite different from typical inorganic nanowires with strong rigidity.^[25] As an upholder to make hybrid nanostructures grow, NiSe_2 UNWs maintained their morphology and ultrathin feature after the second reaction step (Figure 1c). NiO_x NPs with undefined morphology were observed to distribute uniformly on NiSe_2 UNWs. High-resolution TEM (HRTEM) image (Figure 1d) showed about 2 nm diameter of NiSe_2 UNWs and (210) planes with lattice distance of 0.267 nm in NiSe_2 . However, any crystalline structures of NiO_x NPs could not be found by HRTEM and just some darkness with enhanced contrast (circled in Figure 1d) appeared around NiSe_2 UNWs, which suggested that NiO_x NPs might be in amorphous state. NiO_x NPs were synthesized in the same condition and exhibited undefined morphology according to the TEM images (Figure S2a,b, Supporting Information). The X-ray diffraction (XRD) pattern (Figure S2c, Supporting Information) demonstrated the amorphous feature and the X-ray photoelectron spectroscopy (XPS) of Ni 2p region (Figure S2d, Supporting Information) illustrated that Ni was in oxidation state.^[26] Time-dependent control experiments exhibited the formation process of the NSWANs (Figure S3, Supporting Information). With time prolonging, NiO_x grew up from ultrasmall nanoclusters on NiSe_2 UNWs and there were hardly any changes after 12 h. Moreover, temperature-dependent control reactions (Figure S4, Supporting Information) demonstrated that NiO_x would crystallize gradually when the reaction temperature was beyond 120 °C while NiSe_2 UNWs would be cladded integrally by NiO_x with film-like structure when the reaction temperature was below 120 °C.

The crystalline structures of the NSWANs and NiSe_2 UNWs were characterized by XRD. The two patterns (**Figure 2a**) had almost no differences and were both indexed to cubic NiSe_2 (JCPDS No. 11-0552), which further confirmed that NiO_x NPs were in amorphous state. The elemental compositions of NSWANs and NiSe_2 UNWs were determined by inductively coupled plasma-atomic emission spectroscopy (ICP-AES). As shown in Table S1 (Supporting Information), the atomic ratio of Ni/Se in NiSe_2 UNWs was extremely close to 1/2. As for the NSWANs, the atomic ratio of Ni/Se was increased to 1/1, which indicated that the amount of NiO_x NPs might be equivalent to that of NiSe_2 UNWs in the NSWANs. The energy-dispersive X-ray spectroscopy (EDS) in Figure S5 (Supporting Information) also manifested the elemental composition in the NSWANs

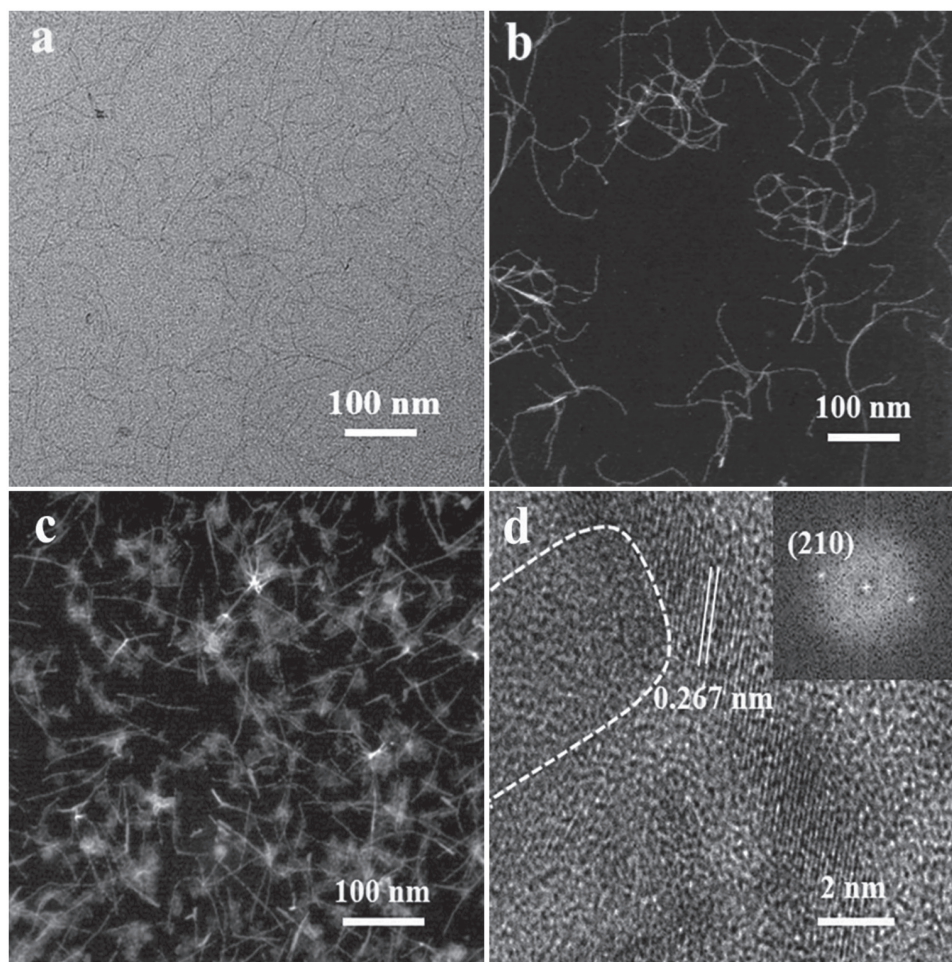


Figure 1. a) Typical TEM image and b) STEM image of the NiSe₂ UNWs. c) STEM image and d) HRTEM image of the as-prepared NSWANs. The inset in (d) is fast Fourier transform pattern of NiSe₂ UNWs. The amorphous NiO_x NPs are circled by the short dashed lines in (d).

and NiSe₂ UNWs. The ratio consequences from EDS results (Table S2, Supporting Information) were identical with that of ICP-AES.

In-depth analyses into surface chemical composition and elemental bonding situation for NSWANs and NiSe₂ UNWs were obtained by XPS and the synchrotron-radiation-based extended X-ray absorption fine structure (EXAFS), respectively. As shown in Figure 2b, the two peaks of NSWANs and NiSe₂ UNWs at 853.2 eV were assigned to Ni 2p_{3/2} orbitals in NiSe₂.^[26] The peak with higher intensity at 855.6 eV in NSWANs was attributed to the Ni in NiO_x NPs while the small peak at the same position in NiSe₂ UNWs suggested the weak surface oxidation.^[27] The Se 3d peaks in XPS spectrum (Figure S6, Supporting Information) at 54.6 eV represented Se in NiSe₂ and the peaks at 59.5 eV were indexed to surface Se species of SeO_x.^[19] Meanwhile, we investigated the bonding situation of Ni in NSWANs and NiSe₂ UNWs through EXAFS. Table S3 (Supporting Information) summarized the structural parameters of the bond lengths, the coordination numbers, and the Debye–Waller factors. Figure 2c presented *k*³-weighted Fourier transform (FT) profiles of EXAFS at Ni K-edge of NSWANs, NiSe₂ UNWs, and NiO, NiSe as the standard samples for comparison.

For the NSWANs, it was clearly observed that Ni–O bond and Ni–Se bond with 2.03 and 2.35 Å of length, respectively, were the major contribution in the real space. The peaks at ≈2.12 Å for Ni in the first shell of NiSe₂ UNWs were agreed with Ni–Se bond, which was the main bond in NiSe₂ UNWs. According to the intensity of pre-edge and white line peaks in the normalized X-ray absorption near edge structure (XANES) spectrum (Figure 2d), oxidation state of Ni could be reflected in different samples, which was caused by the significant contribution of NiO_x NPs in NSWANs and a small quantity of oxidation species on the surface of NiSe₂ UNWs. All of the above characterizations indicated that the hybrid nanostructures were successfully fabricated and prepared for the potential applications in electrocatalysis.

We investigated HER and OER electrocatalytic activities of NSWANs, NiSe₂ UNWs, NiO_x NPs, and commercial Pt/C, IrO₂/C as contrastive samples with a typical three-electrode configuration in 1 m KOH electrolyte. The calibration of reversible hydrogen electrode (RHE) was exhibited in Figure S7 (Supporting Information) and all of the potentials were reported versus RHE. For HER polarization (Figure 3a), the NSWANs could hold 132 mV of overpotential to support 10 mA cm⁻² of current density, which was

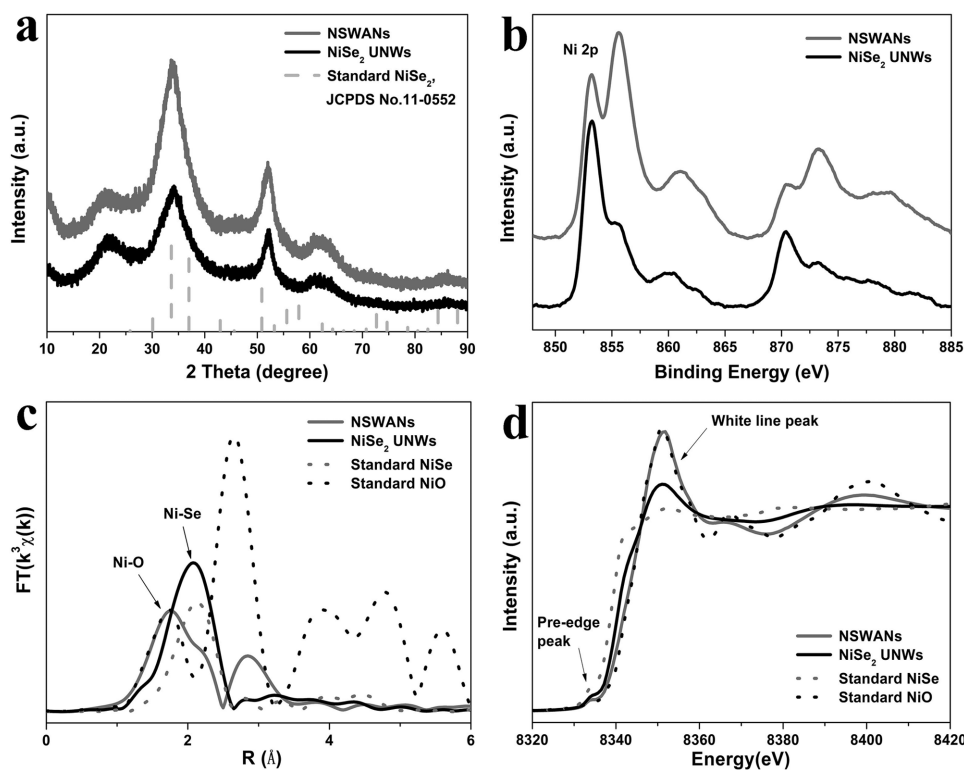


Figure 2. a) XRD patterns of the NSWANs and NiSe₂ UNWs (the dotted lines below correspond to standard cubic phase of NiSe₂ derived from JCPDS card). b) The Ni 2p region of the smoothing XPS spectrum of the NSWANs and NiSe₂ UNWs. c) The k^3 -weighted FT spectra and d) XANES profiles from EXAFS at the Ni K-edge of the NSWANs, NiSe₂ UNWs, and standard NiO, NiSe as contrastive samples.

much better than that of NiSe₂ UNWs and NiO_x NPs. In the meantime, superior kinetics and faster charge transport were achieved over the NSWANs because of their lowest Tafel slope value among the three samples (Figure 3c) and <10 Ω charge transfer resistance (Figure S8, Supporting Information). Even though NiO_x NPs had poorer HER performance than NiSe₂ UNWs, NiO_x NPs could still increase the active sites on NiSe₂ UNWs. We used the double-layer capacitance (C_{dl}) to represent the electrochemical active surface area (ECSA). From cyclic voltammetry (CV) cycles in the range of no Faradaic processes (Figure S9, Supporting Information), we obtained the linear relationship between scan rates and current densities (Figure 3e) and the slope values were the C_{dl} . Obviously, through decorating with NiO_x NPs, the ECSA of NiSe₂ UNWs was enlarged and the NSWANs had the largest ECSA of 253.75 cm² among the three samples for HER. Besides, the NSWANs maintained long-term durability for 24 h at the current density of 20 mA cm⁻² and excellent cyclic stability after 10 000 cycles (Figure 3g, and Figure S10, Supporting Information). To make HER electrolysis more convincing, the comparison between the theoretical amount of H₂ calculated from a chronopotentiometric response at 10 mA cm⁻² for 120 min and the actual production of H₂ experimentally measured from a gas chromatography was shown in Figure S11 (Supporting Information). The result of this comparison indicated that the Faradaic efficiency of HER on the NSWANs was about 100%. Therefore, it was believed that the NSWANs were a valuable electrocatalyst for HER.

The NSWANs also demonstrated the fascinating activity for OER. In the process of OER measurements, the NSWANs just afforded 266 mV of overpotential to deliver 10 mA cm⁻² of current density (Figure 3b). For comparison, higher overpotential of 287 and 310 mV were obtained at 10 mA cm⁻² for NiSe₂ UNWs and NiO_x NPs. Meanwhile, a fast Faradaic process on the NSWANs was exhibited by the smallest Tafel slope and charge transfer resistance of 53.4 mV dec⁻¹ (Figure 3d) and $\approx 18 \Omega$ (Figure S12, Supporting Information), respectively. Owing to the advantage of hybrid nanostructures, the NSWANs owned larger C_{dl} and their ECSA could reach 2094.5 cm² for OER (Figure 3f, and Figure S13, Supporting Information). Figure 3h presented that the NSWANs kept 20 mA cm⁻² activity for 24 h without degradation while only 5 mV upshift was observed on the NSWANs after 10 000 OER cycles (Figure S14, Supporting Information). Because of the complicated process of four-electron reaction, the Faradaic efficiency of OER on the NSWANs could not reach 100% (Figure S15, Supporting Information). The measured values, the theoretical values, and the Faradaic efficiencies at the different periods were summarized in Table S4 (Supporting Information) and the average value of the Faradaic efficiencies was 90.72%.

To make a better understanding of the changes on the NSWANs during the water splitting, we investigated the surface elemental states after OER and HER measurements. As shown in **Figure 4**, the Ni 2p peak at 853.2 eV and Se 3d peak at 54.6 eV could still be seen in the XPS spectra of NSWANs after 1000 OER and HER cycles. The above two

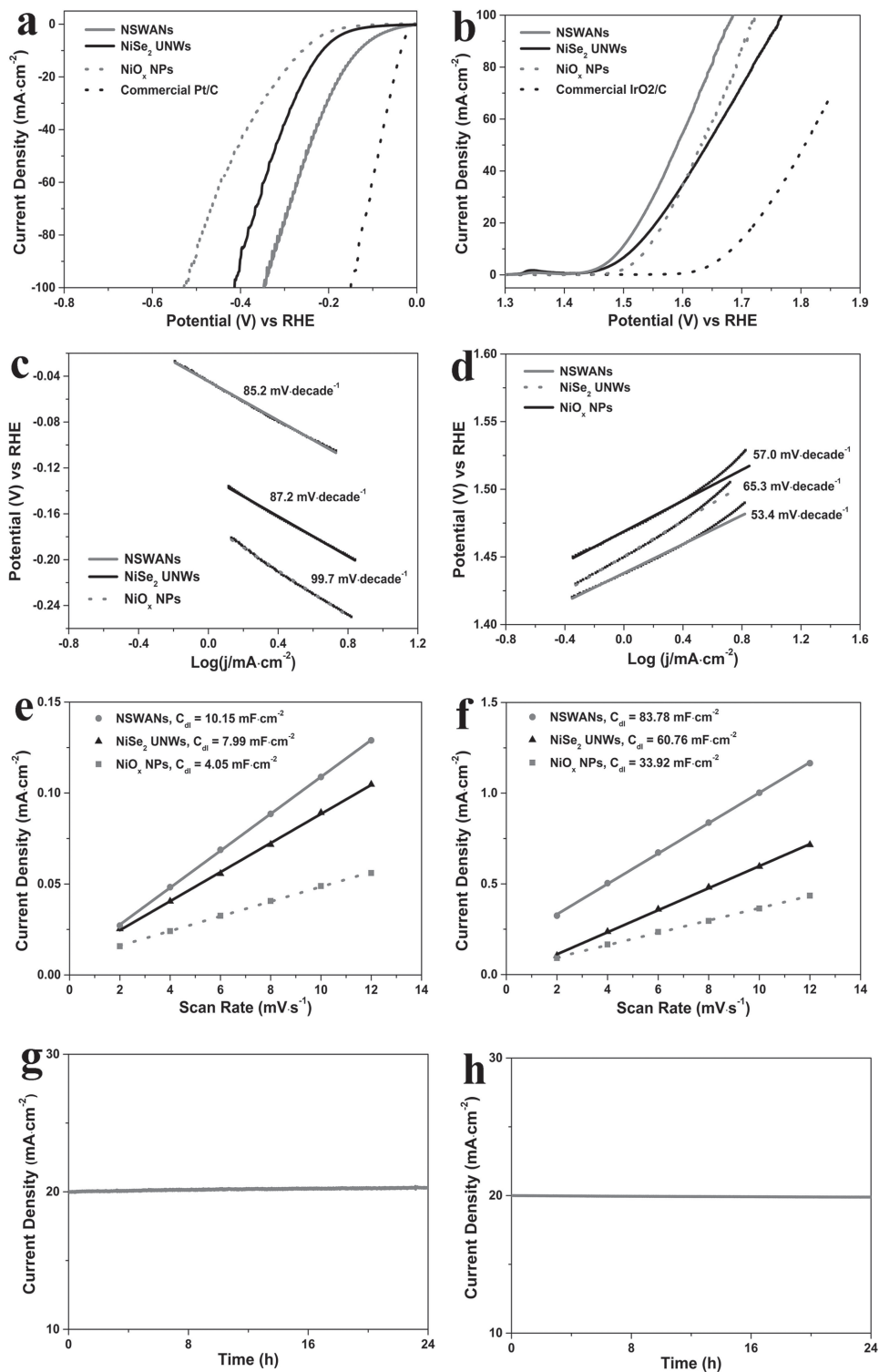


Figure 3. a,b) The polarization curves of the NSWANs, NiSe₂ UNWs, amorphous NiO_x NPs, commercial Pt/C, and commercial IrO₂/C for HER and OER measured in 1 M KOH media at a scan rate of 5 mV s⁻¹. c,d) Tafel plots of the NSWANs, NiSe₂ UNWs, and NiO_x NPs measured at a scan rate of 1 mV s⁻¹ in 1 M KOH media for HER and OER. e,f) The fitting plots showing C_{dl} of the NSWANs, NiSe₂ UNWs, and amorphous NiO_x NPs for HER and OER. For HER, the ECSA of the NSWANs, NiSe₂ UNWs, and amorphous NiO_x NPs were calculated to be 253.75, 199.75, and 101.25 cm², respectively. For OER, the ECSA of the NSWANs, NiSe₂ UNWs, and amorphous NiO_x NPs were calculated to be 2094.5, 1519, and 848 cm², respectively. g,h) Chronoamperometric response curves of the NSWANs for 24 h recorded at a constant applied potential of -0.174 V versus RHE for HER and 1.525 V versus RHE for OER.

positions were indexed to the characteristic peak positions of Ni and Se in NiSe₂. As compared to the NSWANs, the distinct features of NiO_x and SeO_x were demonstrated by

XPS spectra of the Ni 2p and Se 3d orbitals in NiSe₂ UNWs, which indicated surface oxidation of NiSe₂ UNWs after 1000 OER and HER cycles. Besides, we also performed ICP-AES

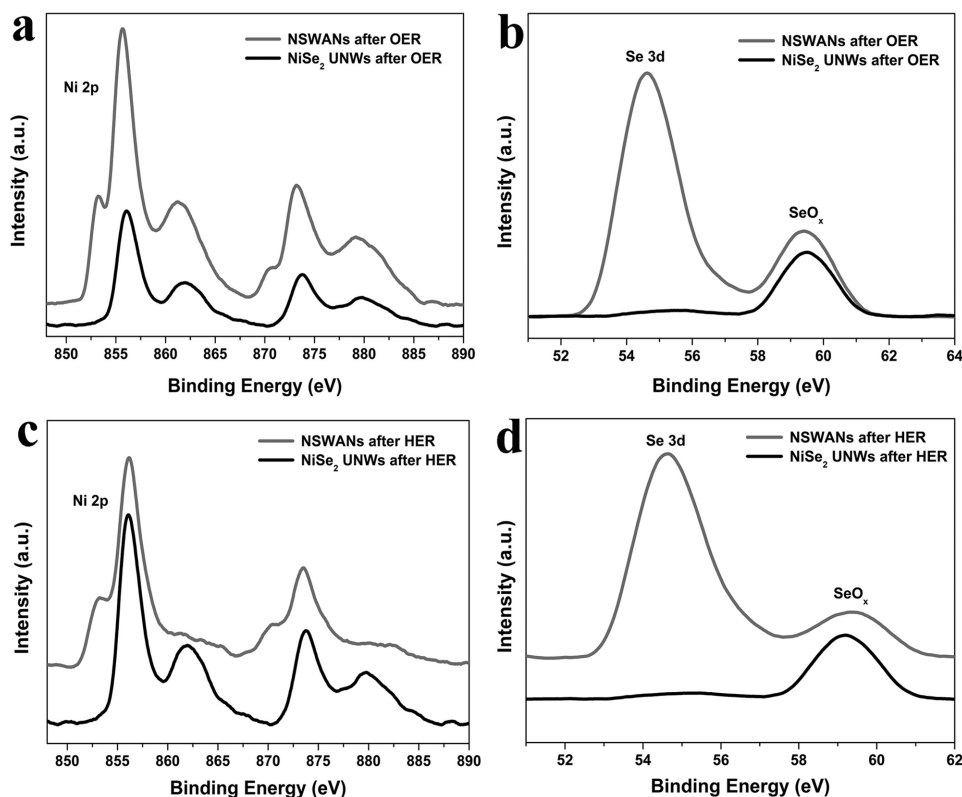


Figure 4. a,c) The Ni 2p and b,d) Se 3d regions of the XPS spectra of the NSWANs and NiSe₂ UNWs after 1000 OER and HER cycles.

measurements to determine the percent proportions of Ni and Se in the NSWANs and NiSe₂ UNWs after OER and HER cycles. Table S5 (Supporting Information) indicated that the content of Ni and Se did not change obviously and Se still existed in the samples rather than dissolving into the solution during OER and HER. As shown in Figure S16a (Supporting Information), the core-shell nanostructure could be observed clearly in the HRTEM image of the NSWANs after 1000 OER cycles. The core material corresponded to NiSe₂, which showed (210) planes with lattice distance of 0.267 nm. The shell structure was marked by the two short dashed lines, which showed the amorphous state and could be matched with amorphous NiO_x. We also carried out the XRD characterization for the NSWANs after 1000 OER cycles. The XRD pattern (Figure S16b, Supporting Information) was indexed to cubic NiSe₂ (JCPDS No. 11-0552). However, the nickel oxides/hydrated nickel oxides could not be observed by XRD, thus demonstrating that the major composition of the NSWANs was NiSe₂ during the OER process. EDS elemental mapping spectra of the NSWANs after OER cycles (Figure S16c, Supporting Information) exhibited the uniform distribution of Ni, Se, and O elements. Meanwhile, EDS spectrum of NSWANs after OER (Figure S16d, Supporting Information) indicated that the atomic ratio of Ni/Se was about 1/1, which further confirmed the ICP-AES result from Table S5 (Supporting Information). Integrating the above consequences, we firmly believed that NiSe₂ cores with a thin NiO_x shell were the active sites during the OER process.

For developing a practical technology, we applied the NSWANs as both cathodic and anodic electrodes

based on CFP with a two-electrode configuration in 1 M KOH media. The overall water splitting current density of 10 mA cm⁻² was produced at an overpotential of only 317 mV on the NSWANs with 1 mg cm⁻² of mass loading (Figure 5a). The NSWANs exhibited evident higher activity than the benchmark combination of commercial IrO₂/C and Pt/C. For the single-component counterparts, they behaved almost the same probably because of the tendency of structural change from NiSe₂ to NiO_x during the electrolysis. Notably, the NSWANs could be polarized for 72 h continuous operation at a current density of 20 mA cm⁻² (Figure 5b). In contrast, the activity of commercial IrO₂/C-Pt/C couple decreased continuously within 7 h (Figure S17, Supporting Information), which was derived from our recent work.^[28] The gas of H₂ and O₂ still evolved on the surface of the two NSWANs electrodes (shown in the digital photo inset Figure 5b) after 72 h operation. Furthermore, an overall water splitting process at a cell voltage of 1.55 V for about 2 min was shown in Video S1 (Supporting Information) based on a two-electrode configuration with the NSWANs, in which a large amount of H₂ and O₂ was released on the left and right electrode, respectively.

In summary, the NSWANs are synthesized by a facile method to form uniform and well-designed hybrid nanostructures. The NSWANs show much better performances for HER and OER than the single-component counterparts, which can ascribe more catalytic active sites and the protective effect of NiO_x NPs on NiSe₂ UNWs. Meanwhile, the NSWANs serve as bifunctional electrocatalysts for overall water splitting exhibiting active and ultrastable

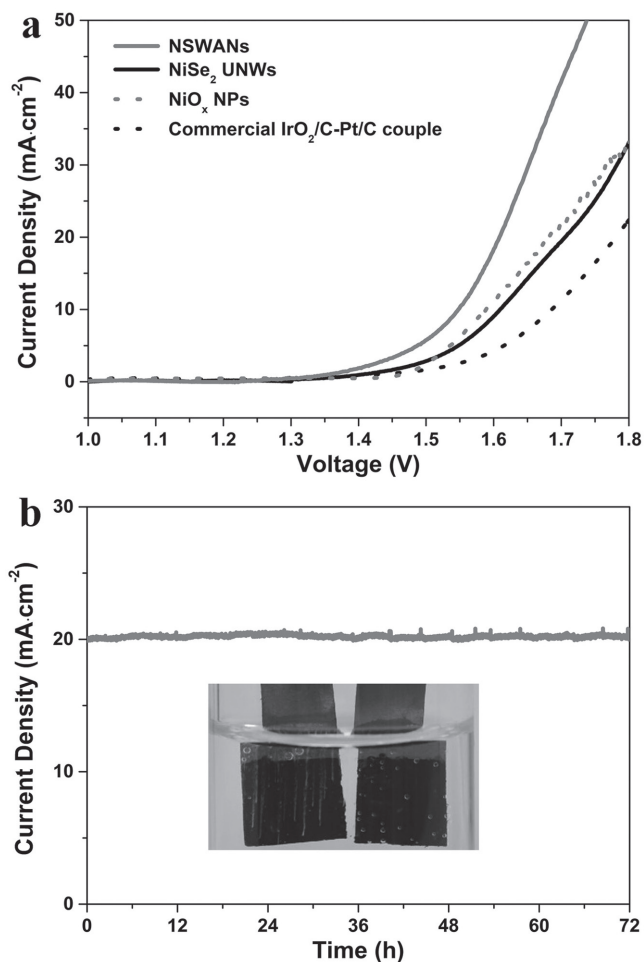


Figure 5. a) Polarization curves of the NSWANs, NiSe₂ UNWs, amorphous NiO_x NPs, and commercial IrO₂/C-Pt/C couple with 1 mg cm⁻² of mass loading in a two-electrode configuration for overall water splitting. b) Chronoamperometric response curves of the NSWANs recorded on a constant cell voltage of 1.6 V. The inset in (b) is a digital photo showing H₂ (on the left electrode) and O₂ (on the right electrode) gas on the NSWANs electrodes after 72 h continuous operation.

features in basic media, which only hold a cell voltage of 1.547 V to reach 10 mA cm⁻² of current density and keep 20 mA cm⁻² activity for 72 h. Our study might help to inspire the development of NiSe₂-based materials in overall water splitting electrocatalysis for practical energy-related applications.

Supporting Information

Supporting Information is available from the Wiley Online Library or from the author.

Acknowledgements

This work was supported by NSFC (21431003, 21521091, 11605201, U1532112), China Ministry of Science and Technology

under Contract No. 2016YFA0202801, and the State Key Project of Fundamental Research for Nanoscience and Nanotechnology (2014CB848900).

Conflict of Interest

The authors declare no conflict of interest.

- [1] a) S. Chu, A. Majumdar, *Nature* **2012**, *488*, 294; b) J. A. Turner, *Science* **2004**, *305*, 5686; c) W. E. Winsche, K. C. Hoffman, F. J. Salzano, *Science* **1973**, *180*, 1325.
- [2] L. Schlapbach, A. Züttel, *Nature* **2001**, *414*, 353.
- [3] a) K. Maeda, K. Teramura, D. Lu, T. Takata, N. Saito, Y. Inoue, K. Domen, *Nature* **2006**, *440*, 295; b) T. E. Mallouk, *Nat. Chem.* **2013**, *5*, 362.
- [4] T. R. Cook, D. K. Dogutan, S. Y. Reece, Y. Surendranath, T. S. Teets, D. G. Nocera, *Chem. Rev.* **2010**, *110*, 6474.
- [5] a) J. Greeley, T. F. Jaramillo, J. Bonde, I. B. Chorkendorff, J. K. Norskov, *Nat. Mater.* **2006**, *5*, 909; b) Y. Jiao, Y. Zheng, M. Jaroniec, S. Z. Qiao, *Chem. Soc. Rev.* **2015**, *44*, 2060.
- [6] a) C. Tang, N. Cheng, Z. Pu, W. Xing, X. Sun, *Angew. Chem. Int. Ed.* **2015**, *54*, 9351; b) H. Wang, H. W. Lee, Y. Deng, Z. Lu, P. C. Hsu, Y. Liu, D. Lin, Y. Cui, *Nat. Commun.* **2015**, *6*, 7261; c) G. Zhang, G. Wang, Y. Liu, H. Liu, J. Qu, J. Li, *J. Am. Chem. Soc.* **2016**, *138*, 14686; d) J. Zhang, T. Wang, D. Pohl, B. Rellinghaus, R. Dong, S. Liu, X. Zhuang, X. Feng, *Angew. Chem. Int. Ed.* **2016**, *55*, 6702.
- [7] a) Z. Lu, L. Qian, Y. Tian, Y. Li, X. Sun, X. Duan, *Chem. Commun.* **2016**, *52*, 908; b) H. Yin, S. Zhao, K. Zhao, A. Muqsit, H. Tang, L. Chang, H. Zhao, Y. Gao, Z. Tang, *Nat. Commun.* **2015**, *6*, 6430.
- [8] a) Y. Jin, H. Wang, J. Li, X. Yue, Y. Han, P. K. Shen, Y. Cui, *Adv. Mater.* **2016**, *28*, 3785; b) Y. Li, P. Hasin, Y. Wu, *Adv. Mater.* **2010**, *22*, 1926.
- [9] a) S. Dou, L. Tao, J. Huo, S. Wang, L. Dai, *Energy Environ. Sci.* **2016**, *9*, 1320; b) Z. Lu, W. Zhu, X. Yu, H. Zhang, Y. Li, X. Sun, X. Wang, H. Wang, J. Wang, J. Luo, X. Lei, L. Jiang, *Adv. Mater.* **2014**, *26*, 2683.
- [10] P. Chen, K. Xu, Z. Fang, Y. Tong, J. Wu, X. Lu, X. Peng, H. Ding, C. Wu, Y. Xie, *Angew. Chem. Int. Ed.* **2015**, *54*, 14710.
- [11] J. Yin, Q. Fan, Y. Li, F. Cheng, P. Zhou, P. Xi, S. Sun, *J. Am. Chem. Soc.* **2016**, *138*, 14546.
- [12] a) P. He, X. Y. Yu, X. W. Lou, *Angew. Chem. Int. Ed.* **2017**, *56*, 3897; b) E. J. Popczun, C. G. Read, C. W. Roske, N. S. Lewis, R. E. Schaak, *Angew. Chem. Int. Ed.* **2014**, *53*, 5427.
- [13] a) T. Y. Ma, J. L. Cao, M. Jaroniec, S. Z. Qiao, *Angew. Chem. Int. Ed.* **2016**, *55*, 1138; b) H. Vrubel, X. Hu, *Angew. Chem. Int. Ed.* **2012**, *51*, 12703.
- [14] a) D. Kong, H. Wang, Z. Lu, Y. Cui, *J. Am. Chem. Soc.* **2014**, *136*, 4897; b) Y. Liu, H. Cheng, M. Lyu, S. Fan, Q. Liu, W. Zhang, Y. Zhi, C. Wang, C. Xiao, S. Wei, B. Ye, Y. Xie, *J. Am. Chem. Soc.* **2014**, *136*, 15670.
- [15] a) M. S. Faber, R. Dziedzic, M. A. Lukowski, N. S. Kaiser, Q. Ding, S. Jin, *J. Am. Chem. Soc.* **2014**, *136*, 10053; b) M. R. Gao, Y. F. Xu, J. Jiang, Y. R. Zheng, S. H. Yu, *J. Am. Chem. Soc.* **2012**, *134*, 2930; c) M. R. Gao, X. Cao, Q. Gao, Y. F. Xu, Y. R. Zheng, J. Jiang, S. H. Yu, *ACS Nano* **2014**, *8*, 3970; d) D. Y. Wang, M. Gong, H. L. Chou, C. J. Pan, H. A. Chen, Y. Wu, M. C. Lin, M. Guan, J. Yang, C. W. Chen, Y. L. Wang, B. J. Hwang, C. C. Chen, H. Dai, *J. Am. Chem. Soc.* **2015**, *137*, 1587; e) M. S. Faber, S. Jin, *Energy Environ. Sci.* **2014**, *7*, 3519; f) M. S. Faber, M. A. Lukowski, Q. Ding, N. S. Kaiser, S. Jin, *J. Phys. Chem. C* **2014**, *118*, 21347; g) M. Cabán-Acevedo, M. L. Stone, J. R. Schmidt, J. G. Thomas, Q. Ding, H. C. Chang, M. L. Tsai, J. H. He, S. Jin, *Nat. Mater.* **2015**, *14*, 1245.

- [16] D. Kong, J. J. Cha, H. Wang, H. R. Lee, Y. Cui, *Energy Environ. Sci.* **2013**, *6*, 3553.
- [17] J. Liang, Y. Yang, J. Zhang, J. Wu, P. Dong, J. Yuan, G. Zhang, J. Lou, *Nanoscale* **2015**, *7*, 14813.
- [18] H. F. Liang, L. S. Li, F. Meng, L. N. Dang, J. Q. Zhuo, A. Forticaux, Z. C. Wang, S. Jin, *Chem. Mater.* **2015**, *27*, 5702.
- [19] F. Wang, Y. Li, T. A. Shifa, K. Liu, F. Wang, Z. Wang, P. Xu, Q. Wang, J. He, *Angew. Chem. Int. Ed.* **2016**, *55*, 6919.
- [20] J. Zhuo, M. Cabán-Acevedo, H. Liang, L. Samad, Q. Ding, Y. Fu, M. Li, S. Jin, *ACS Catal.* **2015**, *5*, 6355.
- [21] L.-A. Stern, L. Feng, F. Song, X. Hu, *Energy Environ. Sci.* **2015**, *8*, 2347.
- [22] a) R. D. Smith, M. S. Prévot, R. D. Fagan, Z. Zhang, P. A. Sedach, M. K. J. Siu, S. Trudel, C. P. Berlinguette, *Science* **2013**, *340*, 60; b) A. Indra, P. W. Menezes, N. R. Sahraie, A. Bergmann, C. Das, M. Tallarida, D. Schmeißer, P. Strasser, M. Driess, *J. Am. Chem. Soc.* **2014**, *136*, 17530.
- [23] H. F. Liang, A. N. Gandi, C. Xia, M. N. Hedhili, D. H. Anjum, U. Schwingenschlögl, H. N. Alshareef, *ACS Energy Lett.* **2017**, *2*, 1035.
- [24] a) E. Tsuji, A. Imanishi, K.-i. Fukui, Y. Nakato, *Electrochim. Acta* **2011**, *56*, 2009; b) R. Nakamura, T. Okamura, N. Ohashi, A. Imanishi, Y. Nakato, *J. Am. Chem. Soc.* **2005**, *127*, 12975.
- [25] a) S. Hu, H. L. Liu, P. P. Wang, X. Wang, *J. Am. Chem. Soc.* **2013**, *135*, 11115; b) B. Ni, X. Wang, *Chem. Sci.* **2016**, *7*, 3978.
- [26] H. V. D. Heide, R. Hemmel, C. F. V. Bruggen, C. Haas, *J. Solid State Chem.* **1980**, *33*, 17.
- [27] M. C. Biesinger, B. P. Payne, A. P. Grosvenor, L. W. M. Lau, A. R. Gerson, R. S. C. Smart, *Appl. Surf. Sci.* **2011**, *257*, 2717.
- [28] H. Y. Li, S. M. Chen, X. F. Jia, B. Xu, H. F. Lin, H. Z. Yang, L. Song, X. Wang, *Nat. Commun.* **2017**, *8*, 15377.

Received: May 9, 2017
Revised: June 19, 2017
Published online: July 26, 2017